Journal of the Meteorological Society of Japan, Vol.79, No.6, pp.1169–1181, 2001

Estimation of Effective Thermal Property Parameter on a Heterogeneous Urban Surface

By Hirofumi Sugawara

Dept. Geoscience, National Defense Academy of Japan, Yokosuka, Japan

Ken-ichi Narita

Dept. Architecture, Nippon Institute of Technology, Saitama, Japan

and

Takehiko Mikami

Dept. Geography, Tokyo Metropolitan University, Tokyo, Japan

(Manuscript received 29 November 1999, in revised form 20 August 2001)

Abstract

A thermal property parameter for expressing the ground heat flux ($c\rho\lambda$; product of the heat capacity and the thermal conductivity) of urban complex terrain was estimated. The surface temperature time series was observed during nocturnal radiative cooling, and employed in the estimation. The surface temperature was obtained using the airborne-measured upward longwave radiation in order to consider the directional anisotropy of radiometric surface temperature. The effective thermal property parameter for a town-scale urban area was found to be two to four times larger than that of the surface material component. The explanation for this, shown by several model simulations and other radiometric observations, was total surface area increased due to urban canyon structure. The parameter $c\rho\lambda$ on the town-scale was expressed by the canyon shape, and the $c\rho\lambda$ of its component material.

1. Introduction

One of the primary causes of the urban heat island phenomenon is the difference in surface heat storage between urban and rural areas. For example, Grimmond and Oke (1999) conducted a study based on observations that the heat storage could exceed 50% of the net radiation as a daily average in an urban area. By numerical simulation, one of the earliest studies showed the importance of heat storage. Atwater (1972) demonstrated that air temperature changes due to urbanization of the soil thermal properties were on a par with changes in other surface parameters, including roughness and moisture availability. However, such numerical studies were based on the thermal property parameters of each surface material, such as urban concrete or rural bare soil. It is not clear whether the thermal property parameter for a large area is equivalent to the averages of each component material. In addition, the parameter of each material composing an urban area has not been determined. In this study, the thermal property parameter of the surface was expressed as $c\rho\lambda$, where $c\rho$ is the heat capacity and λ is the thermal conductivity. Table 1 shows the $c\rho$ and λ of concrete materials reported in previous works. Their variety reaches an order of 100%. Watanabe et al. (1984) showed that concrete thermal property parameters greatly

Corresponding author: Hirofumi Sugawara, Dept. Geoscience, National Defense Academy of Japan, 1-10-20 Hashirimizu, Yokosuka 239-8686, Japan.
E-mail: hiros@cc.nda.ac.jp

Table 1. Heat capacity $c\rho$ and thermal conductivity λ of concrete material shown in the previous works

Source	$c\rho$ $Jm^{-3}K^{-1}$	λ $Wm^{-1}K^{-1}$	$c\rho\lambda$ $J^2s^{-1}K^{-2}m^{-4}$	
Kondo,1994	2.1×10^6	1.7	3.57×10^6	
Astronomical Observatory, 1999	2.0×10^6	1	2.0×10^6	
Matsuo, et al, 1986	1.59×10^6	0.8	1.28×10^6	Artificial light-weight aggregate concrete plate
Matsuo, et al, 1986	1.89×10^6	1.51	2.85×10^6	Ordinary concrete, Pre-cast concrete
Oke,1978	2.80×10^6	0.08	2.24×10^4	Aerated concrete
Oke,1978	2.11×10^6	1.51	3.19×10^6	Dense concrete
Stull,1988	2.26×10^6	2.44	5.51×10^6	
JSME*, 1966	1.7×10^6 ~ 2.0×10^6	0.81 ~ 1.4	0.57×10^6 ~ 2.8×10^6	

*: Japan Society of Mechanical Engineers

depend on the production process and ingredient ratio of the material.

Many studies have addressed earth-surface thermal property parameter estimation. One of the earliest, by Price (1977), demonstrated the thermal inertia ($\sqrt{c\rho\lambda}$) mapping method using satellite data on the surface temperature difference between day and night. The concept was extended to soil moisture estimation (van de Griend et al. 1985). Since those studies appeared, the thermal inertia mapping method has been improved. Xue and Cracknell (1995) used the phase angle information of surface temperature diurnal variation, adding this data to the temperature difference. Sobrino and Kharraz (1999) demonstrated a more sophisticated method that used four consecutive satellite measurements. Hafner and Kidder (1999) applied thermal inertia mapping for the heat island numerical simulation. However, these studies did not solve the problem of directional variations of infrared radiometry. On the heterogeneous complex terrain, the surface temperature has sensor viewing angle dependency. Takamura et al. (1996) showed, using airborne observations, that urban anisotropy of infrared radiometry would cause serious error on radiation budget estimation. The application of these thermal inertia mapping methods were therefore restricted to the homogeneous flat surface (Sobrino and Kharraz 1999). This problem was one focus of the present study.

The main objective of this study is to estimate the $c\rho\lambda$ of a large urban area, laying the groundwork for discussion of the temperature difference between urban and rural areas (heat island intensity). It is helpful to introduce the horizontal scale in this study. The order of 1 km of the built-up area was selected as a sum of urban canyon structures. In this study, this town scale surface was treated as a homogeneous rough surface. Thus, the heterogeneity and complex structure would be included in the heat budget parameters. The heterogeneity involved in this parameter is discussed herein.

In addition to obtaining a physical understanding of the heat island phenomena, there was a second reason for selecting town-scale. Currently, some trial studies are undertaken as potential CO_2 emission-and energy-savings plans in urban areas. In this situation, we must consider the surface heat budget of the entire city rather than each small surface, such as building walls.

In atmospheric boundary layer studies, surface heterogeneity and its effect on the atmosphere are currently of great concern. Many studies have focused on the heterogeneous surface heat budget.

Some of these concentrated on the radiometric surface temperature for expressing the sensible heat transfer. Sun and Mahrt (1995) showed that a negative heat transfer coefficient arises if an adequately defined surface temperature is not used. Matsushima and Kondo (1997) showed that there is a proper nadir angle of the narrow field of the view sensor for surface temperature measurements.

In a discussion of the heat budget in complex terrain, there must be a clear definition of "surface". There are many ways to define the surface in urban complex terrain (Voogt and Oke 1997), as shown in Fig. 1. Once we define the surface, surface heat budget parameters should be determined for that surface. For urban complex terrain, Voogt and Oke (1997) introduced the complete urban surface temperature (T_c), which is the surface temperature averaged on all facets of surface obstacles (Fig. 1). They introduced this as an adequate surface temperature; representative of the urban area. From the viewpoint of representativeness, the surface temperature obtained from upward longwave radiation flux (hereafter RF) observed with an airborne dome-type radiometer (T_{RF}) is very similar to T_c. T_{RF} is the area-averaged temperature including roofs of buildings, walls, and streets. We adopted T_{RF} as an adequate surface temperature in the urban surface heat budget. We call it the RF equivalent temperature. T_{RF} is not exactly equivalent to T_c, because T_{RF} has a biased view factor toward horizontal surfaces and directly beneath the sensor (Voogt and Oke 1997). In this study, averaging along the airborne flight path was conducted to avoid this bias. There were two reasons for adopting T_{RF}. First, we put stress on the surface heat budget. The longwave radiation flux accounts for about the same amount as the sensible heat flux, or the latent heat flux. Second, from the viewpoint of sensible heat transfer, the well-exposed surface should be strongly weighted when obtaining the area-averaged surface temperature. T_{RF} gives the most weight to the fully exposed building roof surfaces. In this study, we define the surface in urban complex terrain by using T_{RF} (Fig. 1), and call it the effective surface contributing to the RF. The $c\rho\lambda$ was estimated and discussed for this defined surface. Under other surface definitions, it is not certain whether the $c\rho\lambda$ estimated in this study would be valid.

The procedure of this study is as follows. First, $c\rho\lambda$ is estimated from the nocturnal cooling time series of RF equivalent surface temperature, which

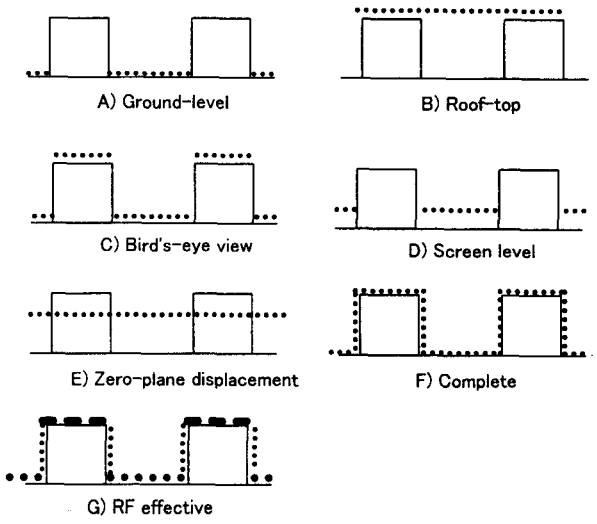

Fig. 1. Definitions of surface in urban canyon structure. A–F are the modified sketch of Voogt and Oke (1997). The RF effective surface (G) is defined in this study.

was obtained by airborne remote sensing observation. Second, more accurate estimation is performed with a one-dimensional heat transfer equation and more frequently observed radiometric surface temperature. Finally, $c\rho\lambda$ is analyzed with the urban canyon structure data.

2. Surrface thermal property parameter ($c\rho\lambda$) for urban surface

The $c\rho\lambda$ of urban complex terrain was estimated from the surface temperature time series. Surface temperature was obtained by airborne remote sensing. Nocturnal cooling time series was needed for the estimation, however the night flight was prohibited for its danger. Therefore, data were obtained at evening and morning. From this restriction, we used the simple method to estimate the $c\rho\lambda$.

2.1 Airborne remote sensing observation

Airborne observation was conducted on October 23 and 24, 1997, in Sapporo, one of the largest cities in Japan. Two consecutive flights were conducted. The first was just before sunset (16:30 JST), and the second was just before sunrise (06:00 JST) the next morning. Weather conditions were fine, and the sky was approximately 1/8 covered with cirrus clouds. The wind speed at urban roof level had been lower than 2.0 ms^{-1} during the night.

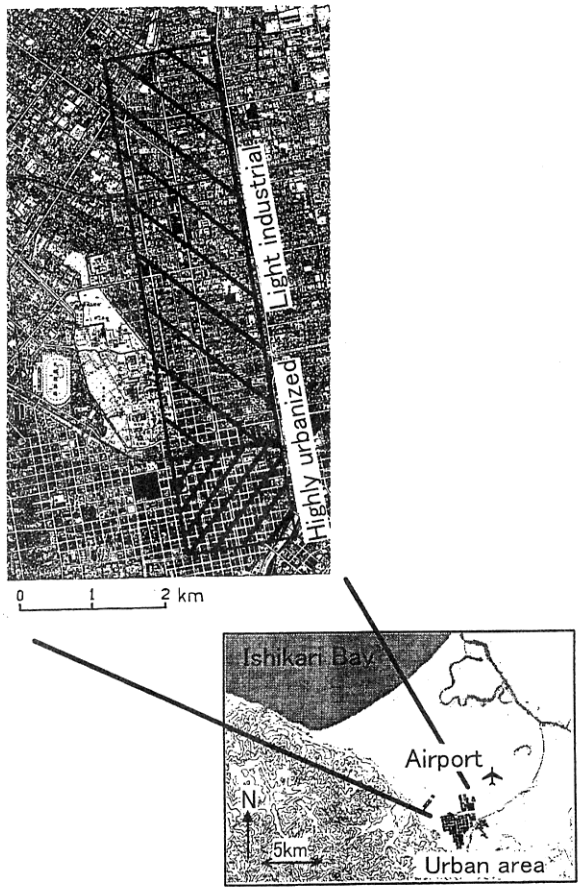

Fig. 2. Target area of the airborne observation in Sapporo. Deep and light shadings represent the highly urbanized area and the light industrial area respectively.

The target area is shown in Fig. 2. The average ratio of building height and street width was 0.78 for the highly built-up area, 0.36 for the light industrial area. The surface temperature was measured for these two different land-covers. In addition, the homogeneous asphalt surface of the airport was measured when the airborne vehicle was landing. As a surface temperature sensor, a pyrgeometer (Eppley PIR, 4–50 μm) was set in an open hatch of the helicopter. It viewed the wall surface as well as the building roof and street, and averaged the three-dimensional urban surface. The flight altitude was 610 m; therefore, the upward radiation flux from the 730 m-radius surface area below the helicopter occupied 80% of the radiation flux at the pyrgeometer. The pyrgeometer dome correction was performed with the dome surface temperature (Shiobara and Asano 1992). Air temperature, air pressure, and humidity were also measured to correct the atmospheric influence on radiation transfer. The correction was done by LOWTRAN7 (Kneizys et al. 1988). Figure 3 shows the validation of the atmospheric correction. The upward radiation profile was measured over the sea surface of Ishikari Bay and compared with the calculation by LOWTRAN7. The observation was conducted during the other observation campaign on 3 Aug. 1996. The weather conditions were calm but cloudy, and the sea surface could be considered to represent thermal isotropy and steady state during the observation period (15 minutes). The difference between the observation and calculation (LOWTRAN7) was larger at a long vertical distance, but at lower than 1.2 km, the mean difference was 1.8 Wm^{-2}.

The measurement error with regard to the dome-corrected pyrgeometer itself was 2.0 Wm^{-2} as a systematic error, and 5.9–10.2 Wm^{-2} as a random error (Shiobara and Asano 1992). These two error factors of instrument and atmospheric correction were considered; therefore, the total systematic error of surface temperature would be 0.6–2.4 K, and total random error would be 0.3–1.0 K.

The pyrgeometer on the airborne vehicle measured the surface temperature average, putting the most weight on the area that was directly below it. The weight became smaller in regions of measurement farther from the point directly below the airborne vehicle. This weight distribution could create a serious error for the measurement of temper-

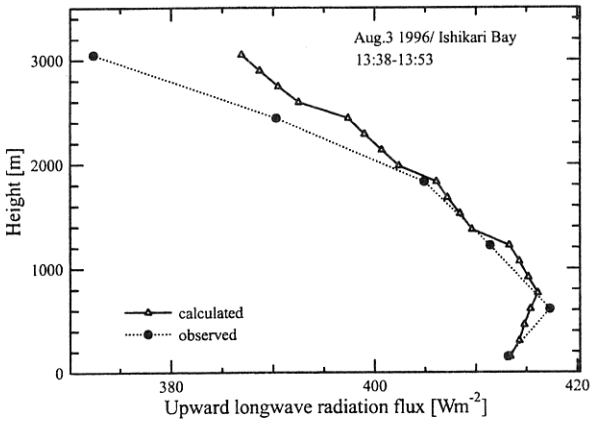

Fig. 3. Validation of atmospheric correction for the airborne pyrgeometer observation. Closed circle is the observed upward longwave radiation over Ishikari Bay. Triangle is that calculated by LOWTRAN7.

ature on the heterogeneous surface. In this study, upward longwave radiation flux was averaged over the flight path to avoid this error. The surface emissivity was assumed to be 1 (blackbody), which should not generate a considerable error in the temperature difference between evening and morning. The validation will be shown later (Section 3.4).

2.2 Results and discussion

Because only two flights were conducted on one night, a simple method was used to estimate the $c\rho\lambda$. The actual cooling amount (δT_{obs}) of the surface temperature in one night was obtained from the data from two successive flights. To compare δT_{obs}, the cooling amount was calculated (δT_{calc}) with assumed $c\rho\lambda$ after Groen (1947) (see also Kondo 1994), as

$$\delta T_{calc} = \delta T_{\max} P(x), \tag{1}$$

$$\delta T_{\max} = T_0 - \left(\frac{L_{sky}}{\sigma}\right)^{1/4}, \tag{2}$$

$$P(x) = 1 - \exp(x)\left\{1 - \frac{2}{\sqrt{\pi}}\int_0^x \exp(-y^2)dy\right\}, \tag{3}$$

$$x = \frac{(4\sigma T_0^3)^2 t}{c\rho\lambda}, \tag{4}$$

where σ is the Stefan-Boltzmann constant. L_{sky} is the downward longwave radiation flux, t is the time from evening, T_0 is the surface temperature at $t = 0$ and $\delta T_{\max}$ is the maximum cooling amount. Solving the one-dimensional underground heat transfer equation under the nocturnal radiative cooling condition yielded these equations. In these equations, sensible heat flux and latent heat flux were neglected. Anthropogenic heat release was also neglected. In obtaining these equations, a constant ground temperature profile was adopted for the initial condition. The calculation of δT_{calc} was performed for different $c\rho\lambda$, although L_{sky} and T_o were determined from observation. The $c\rho\lambda$ that showed the minimum difference between δT_{calc} and δT_{obs} was adopted as an estimation result. The estimation error of $c\rho\lambda$ would then be caused by observation error of L_{sky} and δT_{obs}, which would be $10\,\mathrm{Wm^{-2}}$ and 1 K, respectively. Therefore, the total $c\rho\lambda$ error range would be $3.6 \times 10^6\ \mathrm{J^2\,s^{-1}\,K^{-2}\,m^{-4}}$. For the asphalt surface of the airport, the error range would be narrower because the atmospheric correction would be more accurate at a lower flight altitude.

Table 2 summarizes the results. The homogeneous asphalt surface was almost the same as those in previous works (Table 1). The urban $c\rho\lambda$ was larger than that of the homogeneous asphalt surface or the pure concrete material. Apart from its absolute values, what we have to pay attention to is that the urban $c\rho\lambda$ was larger than that of the flat asphalt surface of the airport. The main reason for the larger $c\rho\lambda$ should be the canyon structure of the urban surface. It is well known that the canyon structure prevents nocturnal cooling, and the temperature fall is slower than that of the fully exposed surface (Oke 1981). The net radiation loss on the surfaces of walls and streets is smaller than that of roofs, because other urban canopy walls covered the former. The resulting $c\rho\lambda$ should be due to the slow cooling rate on the canyon surface.

It was shown that the thermal property parameter $c\rho\lambda$ of the urban surface is larger than that of the homogeneous surface. On the other hand, observation errors of L_{sky} and δT_{obs} would cause a $c\rho\lambda$ error of approximately $3.6\times10^6\ \mathrm{J^2\,s^{-1}\,K^{-2}\,m^{-4}}$. This result is far from satisfactory as a heat budget parameter estimation. Because only two measurements were conducted, it was considered that they could have been much affected by random errors. In addition, there were several insufficiencies

Table 2. Estimation results of the observation with the RF equivalent surface temperature.

Observation area/Source	$c\rho\lambda$ ($\mathrm{J^2s^{-1}K^{-2}m^{-4}}$)
Highly urbanized area (observation)	8.0×10^6
Light industrial area (observation)	5.2×10^6
Homogeneous asphalt (observation)	1.4×10^6
Previous works (Table 1)	$1.28\sim3.57\times10^6$

with regard to the methodology. First, we assumed L_{sky} as constant in calculating δT_{calc}. However, it should vary with cloud movement. Second, the initial underground temperature was assumed to be constant, though fluctuation occurs. To overcome these problems, covered in the next chapter, more frequent measurements of L_{sky} and surface temperature were conducted. The $c\rho\lambda$ for a highly built-up area was estimated using a revised and more sophisticated surface heat budget model.

3. Surface thermal property parameter ($c\rho\lambda$) estimation using continuous measurement

3.1 Observation

An observation was conducted during the summer of 1998 in Tokyo's metropolitan area. Instruments were located on the roof of a Tokyo metropolitan government building, the height of which was 245 m AGL. An infrared thermal imager continuously measured the surface temperature of the urban areas. The infrared image was recorded automatically every five minutes. A pyrgeometer measured the long-wave downward radiation flux density at minute intervals.

An example of the measured infrared image is shown in Fig. 4a. The areas for analysis are framed. As previously mentioned, the observed surface temperature should be the RF equivalent temperature (T_{RF}), or the complete urban surface temperature (T_c) at least. However we used observed surface temperature that is not adequately averaged like T_c or T_{RF}. Land-cover of the target area included highly built-up commercial and residential buildings, whose averaged canyon aspect ratio (building height/street width) was 0.94. The roof area accounted for 40% of the horizontal area. Table 3 shows a summary of the observation and instrument specifications. For $c\rho\lambda$ estimation, nocturnal radiative cooling was adopted; therefore, three nights of calm weather (wind speed $U < 4\,\mathrm{ms}^{-1}$ at about 100 m above the roof level) and no rainfall conditions were strictly selected from a total of 30 observed nights.

Atmospheric correction was performed for each infrared image. A linear relation was assumed between the observed temperature and the corrected surface temperature for each target-sensor distance (d):

$$T_{corrected} = A(d)T_{observed} + B(d). \quad (5)$$

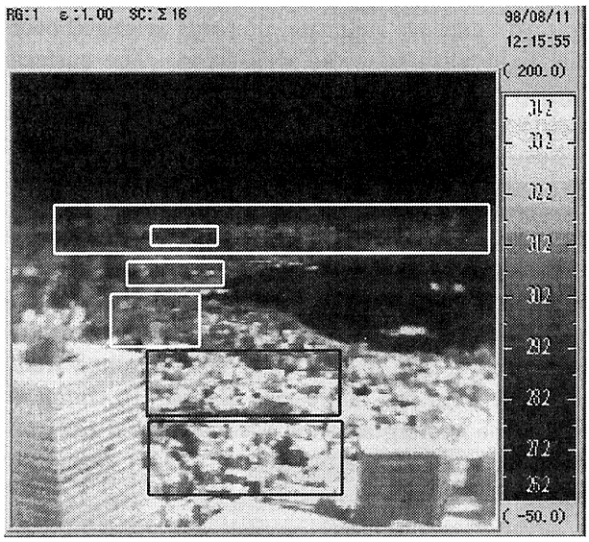

Fig. 4.a) Examples of measured infrared image. Image taken from the metropolitan government building for $c\rho\lambda$ estimation. The areas for the estimation were shown with frame. A low temperature area in the middle right is a forest of Meiji shrine.

Table 3. Details of an observation in Tokyo.

Observation Period	July 26 - August 26, 1998	
Instruments		Measurement interval
Infrared thermal imager	TH3100 (NEC SANEI, Wavelength:8-13 μm, space resolution:1.5mrad, temperature resolution 0.1K, field of view:30×28.5degrees).	5min
Pyrgeometer	PIR (Eppley, wavelength: 4-50μm)	1min
Thermometer, Hygrometer	HUMICAP (VAISALA)	1min
Barometer	PTB100A (VAISALA)	1min
Data logger	THERMODAC-E (ETO DENKI)	

$A(d)$ and $B(d)$ were calculated using LOWTRAN7 with the meteorological data each time.

The atmospheric correction was validated by a moving observation. In the moving observation, the temperature of a given building wall was measured at different distances (100 m–1600 m) from the wall. The specification of the moving observation and an example of infrared images are shown in Table 4 and Fig. 4b, respectively. The observation was conducted around noon, and took 20 minutes. The weather condition was steady, and

the surface temperature measured continuously at the metropolitan government building showed no change during this period. Therefore, we judged it unnecessary to correct the measurement time delay. The averaging was performed, excluding the window on the wall, and the surface emissivity was corrected with Eq.(6).

$$\sigma T_{obs}^4 = \varepsilon \sigma T_{wall}^4 + (1-\varepsilon)\sigma T_{sky}^4, \quad (6)$$

where T_{obs} is the surface temperature observed, T_{wall} is the wall surface temperature, and σT_{sky}^4 is the incident long-wave radiation flux from the sky. The wall surface emissivity ε was determined to be 0.87 from insitu observation for the target wall. T_{sky} was the surface temperature of the sky area in the infrared images. With consideration of the wall surface reflection, σT_{sky}^4 was determined at each distance.

The distance-temperature curve, calculated using LOWTRAN7, is shown in Fig. 5. Error bars represent the temperature variations in the infrared image. The farthest point ($d = 1600$ m) was measured at a Tokyo metropolitan government building. This figure indicates that the calculation has a good accuracy for correcting the radiation temperature. However, at short distances ($d < 150$ m), the uncertainty of emissivity at a low incident angle caused disagreement between observation and calculation. From the radiation transfer, it seems logical to assume that the calculated curve decreased according to the distance; therefore, this disagreement was not a problem of atmospheric correction but of measurement error at moving observation. Except at this shorter range, the total accuracy of surface temperature measurement was 0.6 K.

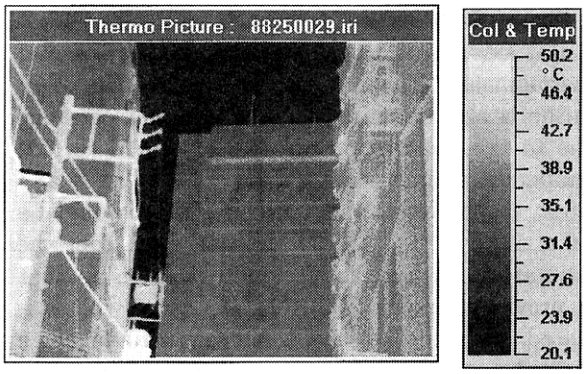

Fig. 4. b) Image at the moving observation. The center building wall is the target of atmospheric correction validation.

Table 4. Details of a moving observation. The weather conditions were measured at the roof of metropolitan government building.

Day	August 25, 1998
Time	13:50 - 14:09
Infrared thermal imager	TVS-610 (Nihon Avionics handy thermometer with battery, wavelength: 8-14μm.
Weather condition during the observation period	Solar radiation: 310Wm^{-2}, Air temperature : 28.8 ℃, Relative humidity: 68%, Air pressure: 973hPa.

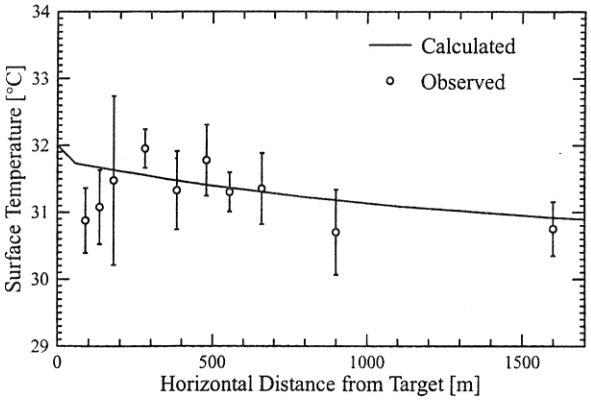

Fig. 5. Validation of atmospheric correction with a moving observation. Open circles are the observed surface temperature. A line is the calculation by LOWTRAN7.

Surface emissivity correction for an urban area is a substantial and difficult problem for surface temperature remote sensing. There are two inhibiting factors: 1) Emissivity of each surface material is still unknown, and appears to have a wide range in urban areas; 2) The incident radiance at the target surface must be known for the correction. However, multiple scattering of longwave radiation in the urban canopy layer is too complex to obtain this value. In this study, we do not deal with each surface of the urban canyon structure, and the surface emissivity on the town-scale was assumed to be 1 (black body). The validity of this value as a surface thermal property estimation will be tested in the next section.

3.2 Estimation methodology

Nocturnal cooling of an urban surface was analyzed and $c\rho\lambda$ was estimated in the following manner. The surface temperature time series was calculated by the surface heat budget model. Calculations were performed with many pairs of assumed $c\rho$ and λ. The best pair of $c\rho$ and λ (i.e., the pair that allowed the minimum difference between the observed and the calculated temperature) was adopted as an estimation result. This method was marked by the fact that the calculation was conducted under real conditions. This was not the case in previous studies, such as that by Sobrino and Kharraz (1999), though this approach is rather similar to that of Hafner and Kidder (1999). The surface heat budget model was used under nocturnal cooling conditions, and the sensible heat flux and the latent heat flux were neglected. The anthropogenic heat flux was not treated explicitly. The surface heat budget can be shown as follows:

$$L_{sky} = G + \sigma T_s^4. \tag{7}$$

L_{sky} is the downward longwave radiation flux at the urban canopy top. G is the ground heat flux, which included the heat flux into the buildings but not canyon air heat storage. The surface emissivity was assumed to be 1 also for the heat budget. A one-dimensional heat transfer equation was used to calculate G.

$$\frac{\partial T}{\partial t} = \frac{\lambda}{c\rho}\frac{\partial^2 T}{\partial z^2}, \tag{8}$$

$$G = -\lambda\left(\frac{\partial T}{\partial z}\right)_{z=0}, \tag{9}$$

where $c\rho$ and λ were assumed to be constant at any depth. In the calculation, time step and vertical grid space were set at 10 seconds and 1 cm. As noted earlier, the urban surface was treated as flat and homogeneous in this study, and a simple boundary condition was therefore adopted. In considering the mean wall depth (30 cm) and daily variation of air temperature, the bottom boundary (50 cm deep) was set at a constant temperature, 27.5 degrees Celsius, which was a one-month average of the observed surface temperature (Jul. 26 to Aug. 26, 1998). The daily temperature cycle does not extend below a certain depth, and the temperature at this depth is almost the same as the daily average of the surface temperature (Stull 1988, P284). Some sensitivity tests indicated that this bottom depth was sufficiently deep, and the lower boundary condition was not so critical. The initial surface temperature condition was set to that observed at 18:00. The underground temperature profile was assumed to be linear between the surface and bottom boundary conditions. This profile is more reasonable than the constant underground temperature condition used in Groen (1947). A trigonometric function would yield a better initial condition; such a function could show the daily variation of the ground temperature profile. However, this method requires additional heat budget parameters, such as the albedo and the sensible heat transfer coefficient. Because these parameters were uncertain for the large-scale surface, the linear initial condition was adopted in this study in order to avoid this uncertainty.

Although $c\rho$ and λ were treated individually, only the product, $c\rho\lambda$, had meaning as an evaluation result. Because $c\rho$ and λ have similar effects on the surface temperature time series, it is impossible to distinguish them using only the surface temperature data in this study. However, we will be able to obtain a significant amount of information useful to distinguishing $c\rho$ and λ when we have conducted a close analysis of the surface temperature time series. It was frequently observed that a quick increase (or drop) in the surface temperature was caused by a sudden increase (drop) of the downward longwave radiation. Moving clouds caused such phenomena, and the surface temperature response may be controlled by the vertical distribution of $c\rho$, λ, and a ground temperature profile. Measurements at adequate intervals will be helpful in estimating these parameters separately, and in obtaining the temperature profile.

3.3 Estimation results and discussion

Figure 6 shows the estimated $c\rho\lambda$. The horizontal axis shows the nadir angle of the infrared thermometer. The $c\rho\lambda$ for the forest of the Meiji shrine is also shown. The estimation error range due to the observation error of L_{sky} and surface temperature time series (T_s) were $10\,\mathrm{Wm^{-2}}$ and 0.6 K, respectively, and total $c\rho\lambda$ error would be $1.0 \times 10^6\,\mathrm{J^2\,s^{-1}\,K^{-2}\,m^{-4}}$. In this case, too, the estimated $c\rho\lambda$ was about twice as large as that in previous reports (Table 1). In Fig. 6, the estimated $c\rho\lambda$ seems to have some sensor nadir angle dependency. There is a slight decrease according to the nadir angle increase. This may be caused by the cooling rate difference between roofs and walls. Their ratio in the sensor field of view would vary according to the sensor nadir angle. This might

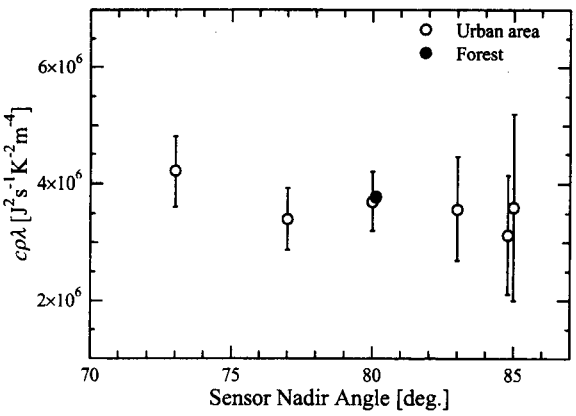

Fig. 6. Estimated $c\rho\lambda$ as a function of the sensor nadir angle. Closed and open circle are forest of Meiji shrine and urban area respectively. The error bar represents standard deviation.

also explain the large $c\rho\lambda$.

These findings raise the question whether anthropogenic heat could be a reason for the larger $c\rho\lambda$. It is possible that the $c\rho\lambda$ estimated in this study included the effect of anthropogenic heat release. However, only the total amount (area total and monthly total) of anthropogenic heat was available under the conditions of the experiment. Generally speaking, investigation is underway regarding anthropogenic heat release; when, where, and how (as sensible heat or latent heat) it is exhausted. Accordingly, it is impossible here to discuss anthropogenic heat quantitatively, and subsequent investigations about canyon structure may contribute to quantitative estimation of anthropogenic heat inversely. Only two points are subjected to qualitative discussion here. 1) Air-conditioning in summer keeps rooms cooler than the outside air. If this has any effect on the outside surface of buildings, it would cause smaller $c\rho\lambda$ (more cooling). Therefore, air-conditioning is not the reason for the larger $c\rho\lambda$. The warm air exhaust from the air-conditioning facilities would not have a direct effect on the building surface temperature and estimated $c\rho\lambda$. 2) If the air-conditioning facilities are running even at nighttime and keeping their respective external surfaces warm, the area-averaged urban surface temperature would show a slow decrease, which would give rise to larger $c\rho\lambda$.

3.4 Validation for black body assumption

We validated the surface emissivity assumption ($\varepsilon = 1$). The surface temperature was emissivity-corrected with the assumed emissivity ($\varepsilon = 0.87$). ε and incident longwave radiation were set as constant for any surface. The $c\rho\lambda$ was estimated from the emissivity-corrected surface temperature, and compared to that from the uncorrected surface temperature. There was only 0.8% difference in $c\rho\lambda$ between them. Therefore the black body assumption ($\varepsilon = 1$) was shown to be practical. The surface emissivity definitely had an effect on the surface temperature time series, but it was negligible in this estimation because the relative time series of the surface temperature was more important than its absolute temperature in $c\rho\lambda$ estimation. It is an advantage of this method that estimation accuracy is depend more on the relative time series than the absolute value.

4. Structure effect in an urban canyon

It was seen in the preceding two different estimations that $c\rho\lambda$ on the town-scale urban surface was larger than that of the component materials. There are two possible explanations for this: anthropogenic heat release, and canyon structure effect. In this section, we examine more carefully the canyon structure effect on the surface thermal property parameter. Quantitative discussions of the two $c\rho\lambda$ estimations will be provided here.

4.1 Canyon structure analysis for continuous observation result

The $c\rho\lambda$ of urban canopy composed of pure concrete surface were simulated for different canyon structures. The surface temperature was simulated and $c\rho\lambda$ was determined for each surface. First we will introduce a simple urban canopy model for nocturnal radiative cooling. Although this is the general model for urban canopy, more stress is required to explain the observation results shown in chapter 3. The urban surface was divided into the wall surface (inside canyon) and the roof surface (outside canyon). The street surface (canyon bottom) was included inside the canyon. The reason for this treatment was that the infrared thermometer field of view (Fig. 4a) did not contain the area constituted by road. The nocturnal cooling of each surface was calculated with Eqs.(7), (8) and (9). An incident longwave radiation $L_{in,wall}$ was determined for the wall surface as follows:

$$L_{in,wall} = SVF_{wall} L_{sky} + (1 - SVF_{wall})\sigma T_{wall}^4. \quad (10)$$

SVF_{wall} is the sky view factor of the walls, and T_{wall} is the wall surface temperature. T_{wall} and SVF_{wall} were represented by the values at the center of the wall (Kobayashi and Takamura 1994). Using Eq.(10), Eq.(7) could be rewritten as

$$SVF_{wall}L_{sky} - SVF_{wall}\sigma T_{wall}^4 - G = 0. \quad (11)$$

A time series of the surface temperatures of the walls and roofs was calculated. Boundary and initial conditions were the same as those in the previous estimation in Section 3.2. L_{sky} was set as a constant ($420\,\mathrm{Wm^{-2}}$). The surface thermal property parameters were set as those of concrete; $c\rho = 2 \times 10^6\,\mathrm{Jm^{-3}\,K^{-1}\,s^{-1}}$ and $\lambda = 1.0\,\mathrm{Wm^{-1}\,K^{-1}}$, after the values set out by the National Astronomical Observatory (1999). Figure 7 shows the simulated wall surface temperature (T_{wall}) for different SVF_{wall}. The wall surface temperature was lower when the wall was more exposed to the sky. The figure also shows the surface temperature that could be measured by infrared thermometer, T_{sens}. T_{sens} is defined as follows in considering the situation that the off-nadir infrared thermometer is set downward-facing the urban canyon:

$$\sigma T_{sens}^4 = \varphi_{wall}\sigma T_{wall}^4 + (1 - \varphi_{wall})\sigma T_{roof}^4. \quad (12)$$

φ_{wall} is the wall view factor of the infrared thermometer, which is defined as the fraction of radiant flux received at the sensor originated from walls. The results in Fig. 7 are easily understood. The radiometric surface temperature depended on

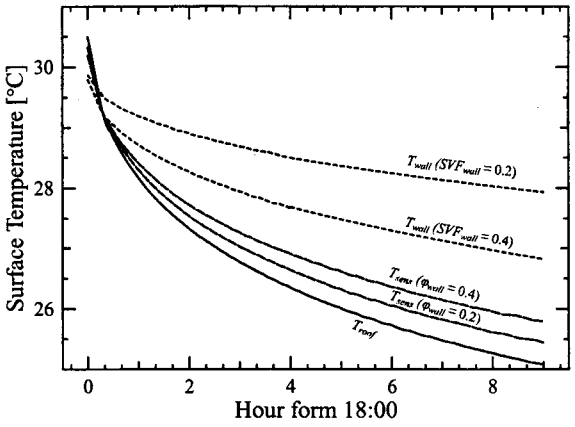

Fig. 7. Calculated nocturnal time series of surface temperature. For walls, a parameter is the sky view factor of wall. For T_{sens}, the sky view factor of the wall was 0.4, and a parameter is wall view factor of sensor.

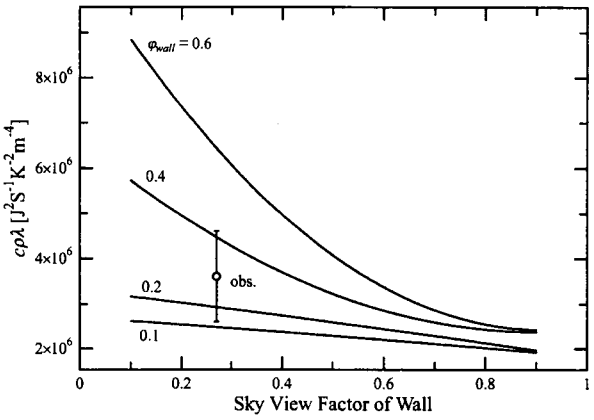

Fig. 8. $c\rho\lambda$ calculated from the simulated surface temperature (line), and that observed (open circle, average of all sensor nadir angle data) with error bar of observation.

the sensor's field of view; what is the purview of the sensor? T_{sens} were located between T_{roof} and T_{wall}, depending on φ_{wall}.

From this calculated surface temperature time series, the $c\rho\lambda$ of urban canopy was estimated inversely in the manner outlined in Section 3.2. The result is shown in Fig. 8, with a horizontal axis representing the sky view factor of wall, SVF_{wall}. Each line shows the different wall view factor of sensor φ_{wall}. $c\rho\lambda$ shows an increase in accordance with φ_{wall}. The surface inside the canyon has less nocturnal cooling; therefore $c\rho\lambda$ should be estimated to be larger when the sensor looks more directly inside the canyon surface. It also increases when the sky view factor of wall decreases; i.e., when there is less nocturnal cooling on the wall.

We shall now look again at a previous estimation result. For the target area of observation, the sky view factor of wall (SVF_{wall}) and wall view factor of sensor (φ_{wall}) were estimated from the building geometry data. For the target area, SVF_{wall} was 0.27 and φ_{wall} was 0.26. Therefore, from the calculation result, it can be said that the $c\rho\lambda$ for the target area could be about 1.5 times larger than the surface component material. The $c\rho\lambda$ observed, an average of $3.6 \times 10^6\,\mathrm{J^2\,s^{-1}\,K^{-2}\,m^{-4}}$ (Fig. 6), was plotted in this figure. For the calculation shown as lines in this figure, the $c\rho$ and λ of each wall and roof were assumed. However, in considering the $c\rho$ and λ range of pure concrete (Table 1), the $c\rho\lambda$ observed was consistent with that simulated within the error range. Therefore we may say that

the reason for the large $c\rho\lambda$ was an effect of the structure.

The canyon structure effect on the $c\rho\lambda$ in complex terrain bears further discussion. This effect can be explained by the fact that more surface area exists in a horizontal unit area; i.e., the total surface area is increased by its three dimensional structure. Therefore, the structure effect on $c\rho\lambda$ can be construed as a correction of the surface area's increase. Moving forward from this study's basic concept, we included the structure effect in the heat budget parameter. If there is twice as much surface area on a horizontal flat surface, and the surfaces do not have any interaction, the heat storage (ground heat flux) on the horizontal unit area will be twice as large as that of the flat surface. In reality, canyon structure causes an interaction between surfaces, and reduces those fluxes to less than twofold. Therefore, an important point is that the resulting $c\rho\lambda$ is valid for the daytime heating process by solar radiation as well as for the nocturnal radiative cooling. The larger surface area should store more heat as an area total.

4.2 Thermal property parameter ($c\rho\lambda$) with RF equivalent surface temperature

To validate the previous estimation result in Section 2.2, $c\rho\lambda$ for RF effective surface was simulated. The application use of $c\rho\lambda$ in a numerical model or surface heat budget analysis will also be considered. The application models designed and investigated in this paper were ones that do not treat the urban canyon structure explicitly.

The methodology used was the same as that in the previous section. The street surface, however, was explicitly distinguished from the walls. For the street (canyon bottom) surface,

$$L_{in,street} = SVF_{street}L_{sky} + (1 - SVF_{street})\sigma T_{wall}^4, \quad (13)$$

$$SVF_{street}L_{sky} + (1 - SVF_{street})\sigma T_{wall}^4 - \sigma T_{street}^4 - G = 0. \quad (14)$$

Here, the RF equivalent surface temperature T_{RF} would be expressed as

$$\sigma T_{RF}^4 = A_r\sigma T_{roof}^4 + (1 - A_r)(\varphi'_w\sigma T_{wall}^4 + (1 - \varphi'_w)\sigma T_{street}^4), \quad (15)$$

where A_r is the fraction of roof area in the target urban area. φ'_w is the wall view factor of airborne pyrgeometer. A_r and φ'_w can be estimated from urban planning data. φ'_w is parameterized using the aspect ratio of urban canyon, H/W (Johnson and Watson 1984),

$$\varphi'_w = (1 - \cos\beta), \quad (16)$$

$$\beta = \tan^{-1}\left(\frac{2H}{W}\right), \quad (17)$$

where H is the building height and W is the street width. The simulation was conducted in the same manner as that in the previous section; i.e., the nocturnal time series of surface temperature was calculated, and $c\rho\lambda$ was inversely estimated from that calculated temperature.

The simulation results are shown in Fig. 9. There was an increase in $c\rho\lambda$ according to the H/W increase and roof area ratio decrease. If there is more roof area, the urban surface acts more like a flat surface and $c\rho\lambda$ is closer to that of the component material. This figure will help us to determine the town-scale $c\rho\lambda$. If we assume the component material $c\rho\lambda$, for example, for an area comprised of concrete, asphalt, and any other material, we can determine the town-scale $c\rho\lambda$ with the building geometry information: A_r and H/W.

Figure 10a shows a comparison of the simulation and the observation results in Section 2.2. Although it shows differences between the results, it indicates also that the main factor for larger $c\rho\lambda$ is the structure effect. There can be several ex-

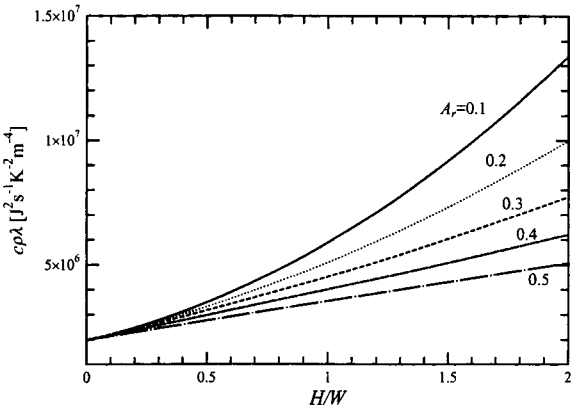

Fig. 9. Estimated $c\rho\lambda$ for the RF effective surface. Horizontal axis is the aspect ratio of urban canyon: building height H and street width W. A parameter is the roof area ratio A_r.

planations for the difference. First, an explanation is anthropogenic heat release. Unfortunately, we cannot thoroughly discuss the anthropogenic heat release due to insufficient data.

The second possible reason would be the green area and open soil surface. Observed $c\rho\lambda$ also showed the large difference in comparison with values from the continuous observation in Tokyo, where no such area was included in the sensor field of view. According to the land-use data, parks and large bare soil surface occupied 10% of the target area. Actually, small gardens should also be counted, adding to this percentage. There was a total of 12.5 mm of rainfall during the 3 days before the observation. For wet soil surface, the $c\rho\lambda$ was reported as 5–6 $\times$ 10^6 $J^2\,s^{-1}\,K^{-2}\,m^{-4}$ (Kondo 1994). Therefore, it is likely that the soil surface at the time of observation may have been in a partially wet condition, which might contribute to a larger $c\rho\lambda$. To evaluate this wet soil condition, the urban canopy with bare soil street was simulated. The $c\rho\lambda$ of roofs and walls were set to the concrete material. Figure 10b represents the case that the streets were bare soil ($c\rho\lambda$ = 6 $\times$ 10^6 $J^2\,s^{-1}\,k^{-2}\,m^{-4}$). These values were about 1.5 times larger than those for the concrete urban canyon. For the light industrial area, wet soil condition could explain well the observed $c\rho\lambda$. On the other hand, for the highly urbanized area, there still exists considerable difference between the observation and the calculation.

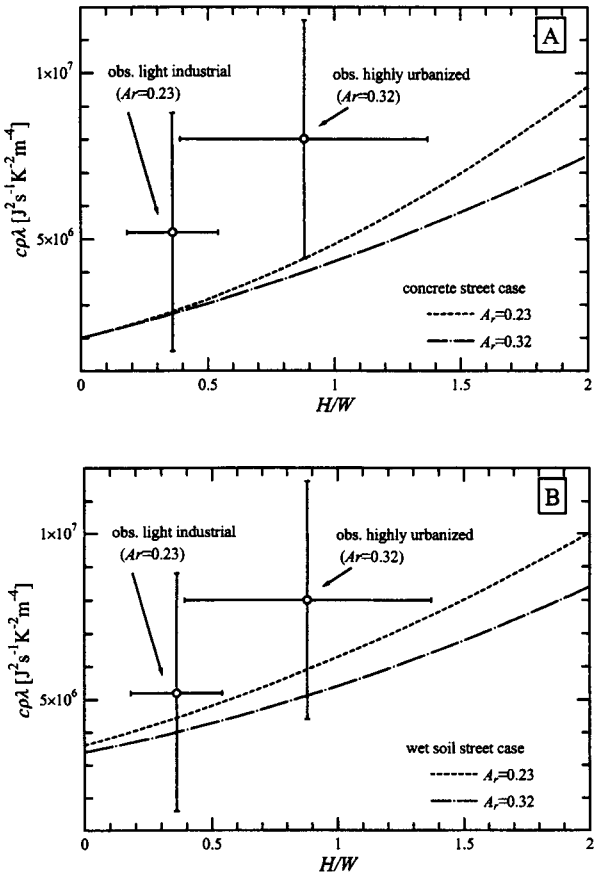

Fig. 10. Comparison between the calculated and observed $c\rho\lambda$ for RF effective surface. a) Calculations are concrete urban canyon condition, and b) wet soil street condition. Horizontal error bar is standard deviation of target area. Vertical one is observation error range.

Although we could not determine a clear explanation for the $c\rho\lambda$ observed for the RF effective surface, we can be fairly certain that the canyon structure effect is a primary factor. Figure 10b indicates that the anthropogenic heat release in the highly urbanized area has a possibility of affecting on $c\rho\lambda$ as a same order as the structure effect. Further investigations should be coupled with investigation of an anthropogenic heat release time series and its distribution within the urban canopy.

5. Conclusion

The parameter for ground heat flux, the product of the heat capacity ($c\rho$), and the thermal conductivity (λ) on a heterogeneous urban complex terrain was estimated. The nocturnal radiative cooling data observed were used with a surface heat budget model. The horizontal scale was set at a few kilometers in order to include the town-scale heat budget analysis and the meso-scale numerical models. To avoid the anisotropy of radiometric temperature, T_{RF} was used for the $c\rho\lambda$ estimation. T_{RF} was defined as the surface temperature equivalent to the upward long-wave radiation flux. This concept is similar to that used to estimate a complete urban surface temperature (Voogt and Oke 1997). T_{RF} was considered in this study to be an adequate surface temperature in the town-scale urban canopy heat budget.

The estimation results demonstrated a $c\rho\lambda$ two to four times larger than that of the surface component material. The simulation using the urban canyon model and more accurate observation indicated that this was mainly due to the urban canyon structure. The heat budget parameter was corrected for the total surface area increase on a complex terrain. It was also shown that the extent

of increase was determined by the canyon structure parameters; the ratio of building height/street width, and the building roof area ratio.

The thermal property of the urban surface has been set to be the same as its component material in many works regarding the urban heat island phenomenon. This study demonstrated that $c\rho\lambda$ should be a few times larger than that of the component material in a bulk model that does not deal with the canyon shape explicitly.

Acknowledgments

The authors thank the Tokyo metropolitan government for their facilitating our observations. Dr. Ushiyama (Kyoto Univ.) gave us a technical advise in the observations. The Japanese Ground Self Defense Force and Prof. Takamura (Chiba Univ.) supported the airborne observation. The observation in Sapporo was facilitated by CRES/ Chiba Univ. The authors also express their gratitude to the helicopter captain, Mr. Kashiwaya, for his help on the night flights. Dr. Naito (NDA) and Dr. Yasuda (Tohoku Univ.) gave us useful comments for the manuscript.

References

Atwater, M.A., 1972: Thermal effects of urbanization and industrialization in the boundary layer: a numerical study, *Boundary-Layer Meteor.*, **3**, 229–245.

Grimmond, C.S.B. and T.R. Oke, 1999: Heat storage in urban areas: local-scale observations and evaluation of a simple model, *J. Appl. Meteor.*, **38**, 922–940.

Groen, P., 1947: Note on the theory of nocturnal radiational cooling of the earth's surface, *J. Meteor.*, **4**, 63–66.

Hafner, J. and S.T. Kidder, 1999: Urban heat island modeling in conjunction with satellite-derived surface/soil parameters, *J. Appl. Meteor.*, **38**, 448–465.

Johnson, G.T. and I.D. Watson, 1984: The determination of view-factors in urban canyons, *J. Climate Appl. Meteor.*, **23**, 329–335.

JSME, 1966: *Dennetsu kougaku shiryou*, JSME, p 258. (in Japanese)

Kobayashi, T. and T. Takamura, 1994: Upward longwave radiation from a non-black urban canopy, *Boundary-Layer Meteor.*, **69**, 201–213.

Kondo, J., 1994: *Meteorology for water environment*, Asakura-shoten, 348 pp.

Kneizys, F.X., E.P. Shettle, L.W. Abreu, J.H. Chetwynd, Jr., G.P. Anderson, W.O. Gallery, J.E.A. Selby and S.A. Clough, 1988: User's guide to LOWTRAN 7. *Air Force Geophysics Laboratory Report*, No. AFGL-TR-88-0177.

Matsuo, Y., S. Murakami, Y. Miyata, M. Kamata and Y. Sakamoto, 1986: *Kenchiku to kishou*, Asakura-shoten. P 22. (in Japanese)

Matsushima, D. and J. Kondo, 1997: A proper method for estimating sensible hat flux above a horizontal-homogeneous vegetation canopy using radiometric surface observations, *J. Appl. Meteor.*, **36**, 1696–1711.

National Astronomical Observatory, 1999: *Chronological Scientific Tables*, Maruzen Co., Ltd., 1058 pp.

Oke, T.R., 1978: *Boundary Layer Climate*, Methuen, London, p 226.

———, 1981: Canyon geometry and the nocturnal urban heat island: comparison of scale model and field observations, *J. Climatology*, **1**, 237–254.

Price, J.C., 1977: Thermal inertia mapping: A new view of the earth, *J. Geophys. Res.*, **82**, 2582–2590.

Shiobara, M. and S. Asano, 1992: The dome emission effect on the performance of pyrgeometers with silicon domes, Pap. *Meteor. Geophys.*, **43**, 17–31. (in Japanese with English abstract).

Sobrino, J.A. and M.H.El. Kharraz, 1999: Combining afternoon and morning NOAA satellites for thermal inertia estimation 1. Algorithm and its testing with Hydrologic Atmospheric Pilot Experiment-Sahel data, *J. Geophys. Res.*, **104 (D8)**, 9445–9453.

Stull, R.B., 1988: *An introduction to boundary layer meteorology*, Kluwer Academic Publ., 666 pp.

Sun, J. and L. Mahrt, 1995: Relationship of surface heat temperature variations: application to BOREAS, *Boundary-Layer Meteor.*, **76**, 291–301.

Takamura, T., T. Kobayashi and H. Sugawara, 1996: Upward longwave radiation and radiation temperature by airborne sensors over urbanized area, *Proceedings of International Radiation Symposium.*.

van de Griend, A.A., P.J. Camillo and R.J. Gurney, 1985: Discrimination of soil physical parameters, thermal inertia, and soil moisture from diurnal surface temperature fluctuations, *Water Resource Research*, **21**, 997–1009.

Voogt, J.A. and T.R. Oke, 1997: Complete urban surface temperature. *J. Appl. Meteor.*, **36**, 1117–1132.

Watanabe, T., K. Himeno and T. Katsuro, 1984: *Proceedings of annual conference of Japan society of civil engineering*, V-222, 443–444. (in Japanese)

Xue, Y. and A.P. Cracknell, 1995: Advanced thermal inertia modeling, *Int. J. Remote Sensing*, **16**, 431–446.